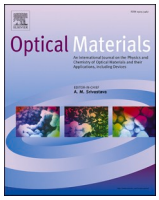
Optical Materials 160 (2025) 116719



Contents lists available at ScienceDirect

Optical Materials

journal homepage: www.elsevier.com/locate/optmat





Photonics in wide-band-gap materials: The challenge of color-center waveguides in lithium fluoride

Rosa Maria Montereali [a,*,1], Valentina Mussi [b], Enrico Nichelatti [c], Massimo Piccinini [a]

[a] ENEA C.R. Frascati, Nuclear Department, Via E. Fermi, 45, Frascati, 00044, Rome, Italy
[b] IMM-CNR, Institute for Microelectronics and Microsystems, Area della Ricerca di Roma Tor Vergata, Via del Fosso del Cavaliere, 100, 00133, Rome, Italy
[c] ENEA C.R. Casaccia, Nuclear Department, Via Anguillarese, 301, S. Maria di Galeria, 00123, Rome, Italy

ARTICLE INFO

Keywords:
Waveguide
Color centers
Photoluminescence
Laser
Lithium fluoride
Photonics

ABSTRACT

Lithium fluoride is an insulating material with outstanding optical properties, among them wide optical transparency. Its ionizing radiation sensitivity allows the formation of primary and aggregate point defects, known as color centers, some of which are laser active in the visible and near-infrared even at room temperature. Among their peculiarities, the simultaneous light emission in the green-red wavelength interval under optical excitation in the blue spectral range is suitable for the realization of solid-state photonic light sources, miniaturized optical amplifiers and lasers compatible with integrated optical circuits. Despite the material's low refractive index, broad-band light-emitting color-center active waveguides were realized at the surface of lithium fluoride crystals and thin films by direct writing with low-energy electron beams and light ions. Due to the complex behavior of radiation-induced defects at high concentrations, the balance between optical gain and losses remains a technological challenge for laser operation. This review will revise the main achievements of our group and emphasize some interesting features, along with a discussion of new experimental results, aiming to promote further developments in photonics and quantum technologies.

1. Introduction

Lithium fluoride (LiF) is an insulating ionic material with outstanding optical properties, among them its wide transparency and very low refractive index [1]. In this face-centered cubic alkali halide crystal, the cation-anion distance, 0.2013 nm, is the shortest. The Li^+ ion and the F^- ion have the smallest radii among the alkali and halide ions, 0.076 and 0.133 nm, respectively. LiF possesses the largest band gap, greater than 14 eV [2], of any inorganic solid and its associated transparency in the deep ultraviolet (UV) region makes it quite a popular optical material. It possesses good chemical stability and high mechanical strength. Its ionizing radiation sensitivity, excellent tissue equivalency and low hygroscopicity promote its commercial use as a dosimeter based on thermoluminescence [3,4], mainly in the form of doped pressed powders. A great extent of bibliography reports on ionizing-radiation-induced production of color centers (CCs) [5,6] in LiF crystals [7–12], some of them suitable for the realization of broad-band, optically pumped lasers operating in the visible and near-infrared, even at room temperature (RT) [13]. The characteristic four-level scheme of CCs makes it possible to obtain population inversion even with low pumping power. Moreover, their peculiar properties, such as spectrally pure photoluminescence (PL), wide continuous tunable bands, very short pulsed regimes and reasonably high powers, were exploited in applied and fundamental research [14,15]. For both the visible-emitting F_2 and F_3^+ aggregate CCs, consisting of two electrons bound to two and three adjacent anion vacancies, respectively, a PL quantum efficiency close to unity was reported [13]. However, the strong overlapping of their broad absorption bands located around 450 nm, known as the M band [7], can reduce the effectiveness of the optical pumping in heavily colored LiF crystals utilized as active media in solid-state lasers. Moreover, other mechanisms of losses, related to re-absorption and/or quenching effects by more complex radiation-induced defects that absorb at the emission wavelengths of the F_2 and F_3^+ CCs, whose broad PL bands are centered at ~678 nm and ~541 nm, respectively, can affect their performances. Simultaneous pulsed laser emission in the green and in the red spectral range [16] was obtained in LiF crystals containing F_2 and F_3^+ CCs at RT with a single pumping wavelength at 450 nm, although their thermo-optical stability under intense laser pumping was limited

* Corresponding author.
E-mail address: rosa.montereali60@gmail.com (R.M. Montereali).
[1] Current address: V. A. Cassani, 39, 00046 Grottaferrata (Rome), Italy.

https://doi.org/10.1016/j.optmat.2025.116719
Received 20 December 2024; Received in revised form 10 January 2025; Accepted 20 January 2025
Available online 22 January 2025
0925-3467/© 2025 The Authors. Published by Elsevier B.V. This is an open access article under the CC BY-NC-ND license (http://creativecommons.org/licenses/by-nc-nd/4.0/).

[17].

Starting in 1988, at the ENEA Frascati Research Center, the search for technologies and methods for the realization of active CC waveguides, which would allow for the development of miniaturized integrated optical amplifiers and/or lasers tunable in the visible, favored the systematic investigation of the properties of stable laser-active CCs emitting in the green-red spectral range produced by low-energy electron beams at the surface of LiF crystals [18,19] and optically transparent thin films [20–23]. The realization of the first CC single-mode channel waveguides in LiF crystals using 12 keV electrons [19] was obtained in the framework of the European ESPRIT project WAFFLE [22], followed by the measurement of amplified spontaneous emission (ASE) of the red light from LiF:F_2 centers [24,25] with significant gain coefficients. Because of these exciting results, low-energy He^+ ions were successfully utilized for the realization of CC multimode waveguides operating in the visible [26–30]. These waveguides are more easily compatible with optical fibers, which typically have a core diameter of few micrometers. Recently, the fabrication of near-infrared single-mode optical waveguides in LiF crystal by carbon ion irradiation [31] was reported.

Starting this century, novel configurations of photonic light-emitting sources based on colored LiF films were investigated for the realization of fully dielectric optical microcavities [32,33] and sub-wavelength miniaturized light sources [34], as well as self-organized nanostructures [35] and single CCs in LiF crystals [36]. Moreover, the peculiar spectroscopic properties of radiation-induced F_2 and F_3^+ CCs, which imply simultaneous emission in the green-red wavelength interval under optical excitation in the blue spectral range, have been successfully exploited in versatile radiation detectors for X-ray imaging in LiF crystals and thin films [37–43], which possess intrinsic high spatial resolution.

In the last 10 years, advanced proton beam diagnostics, Bragg curve imaging and dosimetry have taken great advantages from the visible PL of LiF crystals and films irradiated in different configurations and conditions [44–48] even at clinical dose values used in protontheraphy [49,50]. Concentration PL quenching effects of F_2 and F_3^+ CCs were carefully investigated at high doses [51].

More recently, Fluorescent Nuclear Track Detectors have been demonstrated in LiF crystals [52–54] and are under investigation for applications in radiobiology [55,56], energy and space [57].

All these exciting results were favored by progress in materials science and nuclear technologies, high-performance instrumentation for optical spectroscopy and microscopy [43], as well as impressive advancements in photonics. In this review, we will focus on the main achievements of our group regarding non-hybrid broad-band light-emitting CC active waveguides realized at the surface of LiF crystals by direct writing with low-energy electron beams and bombardment with He^+ ions. They are critically revised and some new experimental results are presented and discussed with the aim of stimulating further research and developments in the growing field of active photonics, among them tunable photonic integrated lasers for hybrid quantum technologies [58] and control of nano-emitters based on CCs in crystalline dielectric media [59].

2. Color-center channel waveguides in LiF crystals by electron beam lithography

Despite the material's low refractive index, broad-band light-emitting CC single-mode channel waveguides were realized at the surface of LiF crystals [19] and thick LiF films grown on LiF crystals [60] by direct writing with low-energy electron beams. The main limitation to the design of the waveguiding structure, even in the thin film geometry, is related to the low refractive index of LiF, 1.3912 at 640 nm [1], which prevents from using the most common substrate materials. The idea is that a spectral dependent increase of the refractive index at the surface of LiF crystals can be locally obtained by the stable formation of a high concentration of CCs, as proposed in Ref. [61] for electrons.

Irradiation with low penetrating particles, such as low-energy electrons or light ion beams, involves only thin surface layers of the bombarded material, within a thickness of the order of a few micrometers or less, as sketched in Fig. 1 for two non-hybrid LiF-based waveguide configurations. For the e-beam irradiation, a shallow volume containing high concentrations of F, F_2 and F_3^+ CCs is created, whose maximum penetration depth d is estimated between 0.15 and 7.3 μm depending on the selected beam energy E from 3 to 30 keV, according to the following semiempirical relation [62].

$$d = \frac{0.064}{\rho} E^{1.68} \quad (1)$$

where ρ is the LiF density, 2.635 g/cm^3. The primary F center, consisting of an anion vacancy occupied by an electron, is the simplest one, and its absorption band is peaked around 248 nm [63]. According to the Kramers-Kronig relations [64], the stable formation of these lattice defects, which absorb in the near UV, induces a spectrally dependent increase of the real part of the refractive index n in the irradiated volume with respect to the unirradiated one at longer wavelengths, that is, in the same spectral interval where the F_2 and F_3^+ visible emission bands are located. A similar index variation can be foreseen for both the F_2 and F_3^+ CCs. Thus, the creation of a densely colored layer in LiF represents a straightforward method for realizing a guiding structure. Higher defect concentrations imply the improvement of the confining properties of the waveguides; on the other hand, at high irradiation doses, the presence of different aggregate CCs causes optical losses due to re-absorption of the emitted photons. Then, the increase in n within the colored region compared to the uncolored one must avoid also increasing k, the imaginary part of the refractive index, to prohibitive values. This ensures relatively low propagation losses, provided that the depth of such a layer is enough to support at least one propagating mode at the emission wavelengths of these defects.

The first CC single-mode waveguides, with strong visible PL in the red and green, were realized by irradiating LiF crystals with low-energy electron beams of 12 keV [19] at a fluence of 8×10^{-3} C/cm^2. The impinging electrons create optically active defects and these induce a change in the LiF refractive index, as explained above. The resulting active waveguides emit and amplify the guided visible light, due to the presence of the laser-active F_2 and F_3^+ CCs. The single treatment transfers a defined waveguide pattern onto the surface. Colored stripes, 15 mm long and 145 μm wide, were realized. The width was chosen large enough to allow using prism coupling and detect possible guided modes, whose propagation constants were measured using the well-known dark-line spectroscopy technique [65]. The colored stripe resulted to be supporting a single mode at different wavelengths, from the blue-green lines (472.7, 488.0, 496.5, 514.5 nm) of the argon laser to the red line (632.8 nm) of the He–Ne laser; from the measurements, an

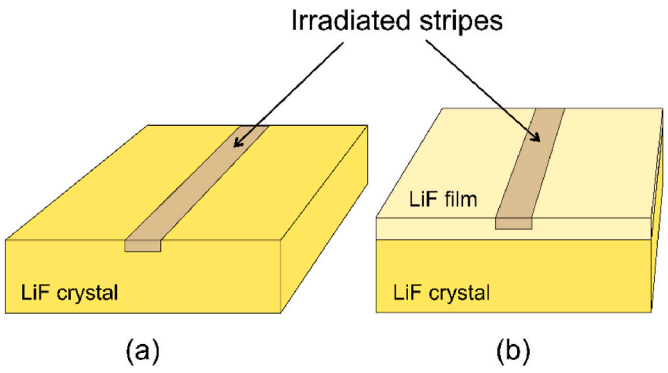


Fig. 1. Scheme (not to scale) of channel waveguides written by e-beams in a LiF crystal (a) and in a LiF film grown on a LiF crystal (b).

increase of refractive index of ~5×10^{-3}, suitable for light confinement, was evaluated. A direct measurement of the propagation losses was prevented by the absence of scattering from the polished LiF crystal surface. When pumped with the 457.9 nm blue line of the argon laser, the samples emitted green and red light, visible to the naked eye (see Fig. 2a).

Under the same electron irradiation conditions, single-mode light propagation, along with intense broad PL in the visible spectral range, was measured in a colored channel induced by electron beam lithography on a polycrystalline LiF film, 3.0 μm thick, grown by thermal evaporation on a polished LiF single crystal, shown in Fig. 2b, kept at a temperature $T_s = 280$ °C during the deposition. Again, the stripe was supporting a single mode at the 632.8 nm line of a He–Ne laser with optical losses of ~6.4 dB/cm, a significant value ascribed not only to the optical absorption of more complex aggregate defects, but also to the polycrystalline nature of the film, due to light scattering at the grain boundaries and possible lack of homogeneity along its thickness [60]. It should be noticed that the realization of a CC waveguide is not automatically assured if one uses for the film-based structure the same irradiation conditions utilized for the LiF crystal. Although the main spectral features of the F_2 and F_3^+ CCs are like the ones in bulk crystals, their formation efficiency is higher in polycrystalline films than in single crystals [66] and depends on the peculiar nature of the films, whose structural and morphological properties are strongly influenced by the deposition conditions and substrate characteristics. Moreover, the surface to volume ratio plays a main role because it is related to the density of the grain boundaries, which act as a source of vacancies during the CCs formation and stabilization processes [67]. This topic belongs to a growing field of research which is out of the aim of this paper.

Treating lithium fluoride crystals and films with an electron beam could produce waveguide lasers and amplifiers tunable across the visible spectrum, depending on the balance between optical gain and losses. Due to the complex zoology of radiation-induced defects created at the high doses utilized for obtaining light confinement, several basic and technical aspects should be carefully investigated. For these reasons, optical gain and absorption measurements were performed on the colored stripes irradiated at increasing doses and two slightly different energies, as listed in Table 1. The mean absorbed dose, defined as the energy deposited per unit mass, is reported in Gy.

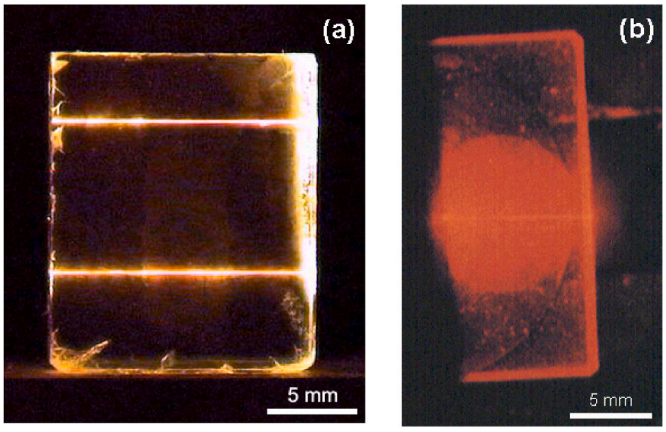


Fig. 2. Photograph of photoluminescent channel waveguides produced with 12 keV electrons at the surface of a LiF crystal by direct e-beam writing, under illumination with blue laser light at 457.9 nm (a). Photograph of He–Ne light propagation at 632.8 nm (coupled by a prism on the left) in a stripe waveguide induced by 12 keV electrons at the surface of a LiF film 3.0 μm thick (round circle) thermally evaporated on a LiF crystal kept at a temperature Ts = 280 °C during the growth (b). (For interpretation of the references to color in this figure legend, the reader is referred to the Web version of this article.)

Table 1
Irradiation conditions of CC channel waveguides realized in LiF crystals with low-energy electrons.

Energy (keV)		12		13
Maximum depth in LiF *d* (μm)		1.58		1.81
Mean energy loss (keV/μm)		7.59		7.18
Fluence (C/cm²)	2.2×10^{-3}	3.3×10^{-3}	8.8×10^{-3}	6.9×10^{-3}
Fluence (e/cm²)	1.4×10^{16}	2.1×10^{16}	5.5×10^{16}	4.3×10^{16}
Mean dose (Gy)	6.3×10^7	9.5×10^7	2.5×10^8	1.9×10^8

2.1. Gain coefficients and laser active defects

Single-mode CC-based active waveguides induced at the surface of LiF crystals by direct writing with low-energy electron beams take peculiar advantages of the unique combination of optical and lasing properties of the electronic defects efficiently generated inside the LiF surface layers and the confinement properties of the selected configuration. The stable formation of high concentrations of primary F and aggregate defects locally induces a spectral modification in the refractive index of the irradiated material: an index increase up to 10^{-3} in the green-red wavelength range is sufficient to confine the laser-active F_2 and F_3^+ visible PL under optical excitation in the blue spectral range. The net optical gain coefficients in irradiated LiF crystals were obtained by measuring the ASE spectra as a function of the pump power density for a fixed length of the stripe waveguides. In terms of gain, ASE occurs when the spontaneous emission from a distribution of inverted systems is amplified by stimulated emission without the help of a resonant cavity to provide feedback and mode structure. Practically, the ASE phenomenon rapidly becomes the predominant decay mechanism for the active medium as its signal intensity increases rapidly with population inversion when the proper threshold conditions for the pump power are exceeded. In these waveguides, the CCs spontaneous PL was amplified as it passed through the waveguide volume by stimulating the PL of the laser excited CCs to reach the polished edge of the crystal. The LiF samples were pumped with the 457.9 nm line of an argon ion laser in quasi-continuous-wave regime at RT using two different geometries between excitation source, waveguide and photomultiplier detector, and the lock-in technique was used. In the *frontal* geometry (see inset on the right in Fig. 3a), the unconfined PL, emitted by the CC waveguide along the direction perpendicular to the crystal surface, was measured: all the spectra consisted of the superposition of the broad emission bands of F_2 and F_3^+ CCs, as shown in Fig. 3a (solid line). In the *perpendicular* geometry (see inset on the left in Fig. 3a), the guided PL exiting through the waveguide end was collected. The spectra, taken as a function of the pump power density in the interval from 0.26 to 0.42 W/cm², showed a narrowing of the F_2 emission band and a strong reduction of the F_3^+ one (see dashed lines in Fig. 3a). By measuring the exponential variation of the PL output as a function of the pump power density at a fixed excitation length *l* of 2.5 mm [25], appreciable values of the gain coefficient, from 3.19 to 4.67 cm^{-1} were obtained for LiF:F_2 at 650 nm. The same exponential behavior was observed for the entire wavelength range from 580 to 730 nm, as one would expect due to the homogeneous broadening of the CCs emission bands. The observed narrowing of the emission band of the F_2 centers, with a reduction of the full width at half maximum (FWHM) up to 83 % when detected in perpendicular geometry, can be ascribed to the ASE phenomenon. On the contrary, no amplification was observed in the green range, probably because of the appreciable presence of parasitic centers, such as the F_4 defects (four aggregate F defects), whose absorption bands at 520 and 545 nm overlap the broad emission of the F_3^+ active centers, as discussed later.

The spectra reported in Fig. 3b were collected in a colored stripe 30 μm wide, realized with a 13 keV electron beam in a LiF single crystal

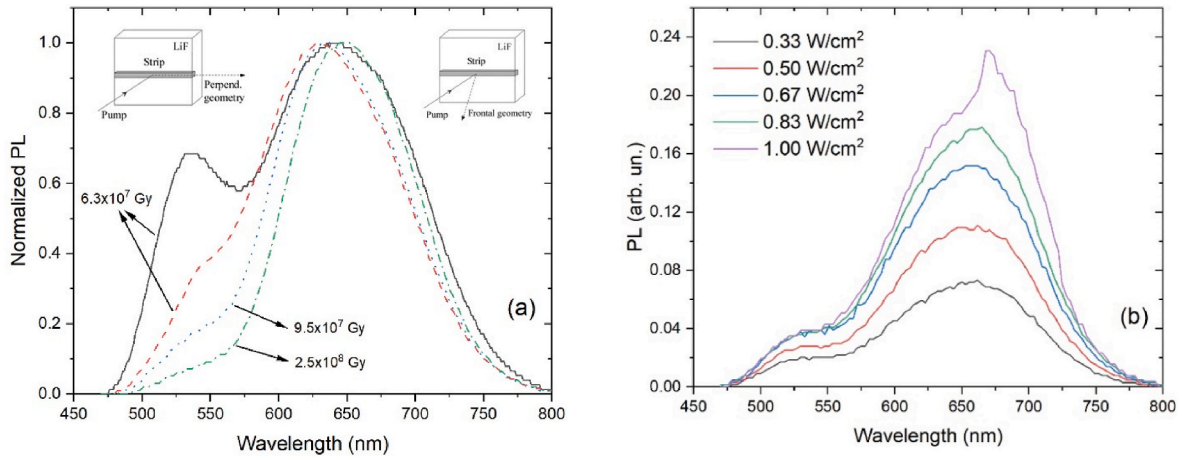


Fig. 3. Room temperature PL (black solid) and normalized ASE spectra of three channel waveguides colored with 12 keV electrons at different doses in a LiF crystal (color dashed), measured under laser pumping at 457.9 nm for an excitation length of 2.5 mm at a power density of 0.31 W/cm^2. The PL collecting schemes are reported as inset (a). ASE spectra of the stripe waveguide colored by 13 keV electrons at a dose of 1.9 × 10^8 Gy in a LiF crystal, measured under increasing laser pump power density at 457.9 nm for an excitation length of 3 mm (b). (For interpretation of the references to color in this figure legend, the reader is referred to the Web version of this article.)

only 4 mm long with a dose of 6.9 × 10^{-3} C/cm^2 (see Table 1), by pumping with the 457.9 nm line of an argon laser in quasi-continuous-wave regime on a length of 3 mm [68] at increasing laser pump power density from 0.33 to l W/cm^2. At this maximum power density, which is well below the saturation intensity of 2.3 × 10^5 W/cm^2 [25], a more intense narrow emission was observed around 670 nm, close to the peak of the F_2 photoemission band. This amplified oscillation is reasonably ascribed to the waveguide laser modes in a nonselective cavity for the presence of limited feedback due to Fresnel reflection (~2.5 %) from the polished edges of the crystal. The narrow peak disappeared when the ASE spectrum was successively recorded in the same conditions. As the spectra were obtained by sequentially acquiring the PL signal with a resolution of 3 nm, the temporal duration of the observed phenomenon was estimated to be around 25 s. The limited thermo-optical stability of the F_2 CCs, which are photoionized under intense pumping [15], giving rise to the F_2^+ (ionized F_2) ones, whose broad absorption, located at 632 nm, strongly overlaps with the F_2 emission [69] can explain the observed behavior.

Then, in the CC waveguide configuration, limited feedback is sufficient for the F_2 laser action even at low power density. It should be considered that these defects possess the largest Stokes shift among the various laser active CCs in LiF and they should also provide the largest gain for a given pumping level, being the amplifier scheme the nearest to a pure four-level one. In a homogeneous medium containing CCs, the gain coefficient g is due to the interaction between the defect and the lattice. In absence of non-radiative phenomena, it is described by the same shape as the emission band and the following formula [14] is valid:

$$g(\lambda) = \sigma_e(\lambda) N_{RES} \tag{2}$$

where σ_e is the emission cross-section and N_{RES} is the pumped F_2 population in its excited state. For a Gaussian band, at the resonance wavelength λ_e, σ_e is given by the following expression:

$$\sigma_e(\lambda_e) = \frac{\lambda_e^2 \cdot \eta}{8\pi \cdot n^2 \cdot 1.064 \cdot \tau \cdot \Delta\nu} \tag{3}$$

where $\Delta\nu$ is the FWHM of the emission band, n is the refractive index of the medium at the resonance wavelength, τ is the luminescence lifetime and η is the luminescence quantum efficiency. For the experimental conditions described, N_{RES} is directly proportional to N_0, the ground state population, i.e., the concentration of F_2 centers, according to the following equation,

$$N_{RES} \sim \sigma_a(\lambda_p) N_0 \tau \phi \tag{4}$$

where σ_a is the absorption cross section at the pumping wavelength λ_p and ϕ the pumping photon flux. For Gaussian bands, calculation of cross-sections for absorption and emission of F_2 center gives the spectra shown in Fig. 4a, according to the values reported in Table 2 for the F_2 and F_3^+ laser active defects [10,69]. An oscillator strength of 0.28 was used for the calculation of the absorption cross section using the Smakula's equation [5]. In Fig. 4a the complete absence of spectral overlapping between absorption and emission indicates a pure four-level scheme for amplification.

It should be noticed that the values derived for the gain coefficients from the ASE spectra of the three stripe waveguides colored with 12 keV electrons were found to be increasing with the electron irradiation dose, as shown in Fig. 4b: higher doses induce higher defect concentrations, which imply the improvement of the confining properties of the colored stripes due to a greater increase in the real part of the refractive index in the irradiated LiF region. Moreover, according to equations (2) and (4), a higher density of F_2 centers directly contributes to rising the gain coefficient, which increases linearly with the population inversion of the defects responsible for the emission. The behavior in Fig. 4b can be best-fitted using an elementary model that predicts a linear growth of the CC density N_0 vs. dose, followed by a saturation stage at high doses. This model has already been applied to describe the PL of radiation-induced F_2 CCs in LiF films [45] and crystals [46,51] irradiated with 3 MeV energy protons, assuming a direct proportionality between N_0 and the PL intensity emitted by the CCs. The saturation dose D_0 is defined as a threshold dose value above which saturation begins to be evident. From the best-fit of the data points in Fig. 4b, a saturation dose $D_0 = 5.5 \times 10^7$ Gy was obtained. This value provides a useful information about the suitable irradiation conditions for laser action in the case of low-energy electron beams.

The small width of the engraved CC stripe waveguides makes it difficult to directly measure the normal-incidence optical transmittance of the sample. Only thanks to the development of a versatile spectrophotometer [70], near-normal optical transmittance spectra of the channel waveguides produced in LiF crystals with low-energy electrons, at irradiation conditions very similar to those reported in Table 1, were measured. The corresponding optical absorption spectra are shown in Fig. 5a along with the one of a blank crystal. Besides the main bands, due to F and M absorptions, other features associated to the presence of different types of aggregate defects were detected. Among them the 315

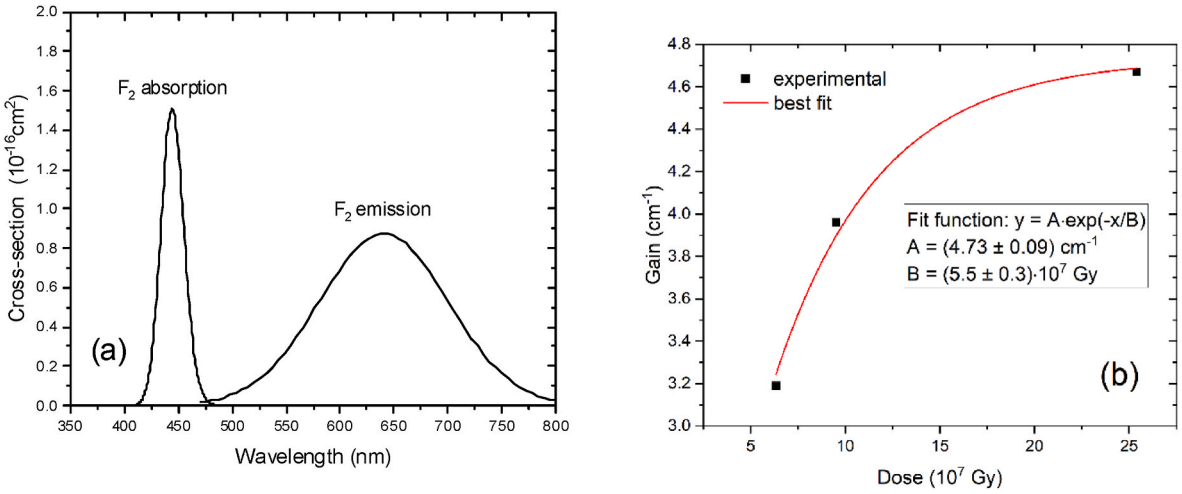


Fig. 4. Absorption and emission cross-sections for F_2 CCs in LiF at RT (a). Gain coefficients measured at 650 nm on the three stripe waveguides colored by 12 keV electrons in a LiF crystal as a function of the irradiation dose. A best fit (solid line) is also shown (see the text for details) (b).

Table 2
Spectroscopic properties at RT of laser active F_2 and F_3^+ color centers in LiF.

CCs in LiF	λ_a (nm) E_a (eV)	$\Delta\nu_a$ (10^{13} Hz) *FWHM$_a$ (eV)*	λ_e (nm) E_e (eV)	$\Delta\nu_e$ (10^{13} Hz) *FWHM$_e$ (eV)*	τ (ns)	η (%)
F_2	444	3.3	678	7.5	17.2	100
	2.79	0.16	1.83	0.36		
F_3^+	448	6.1	541	6.5	11.5	100
	2.77	0.29	2.29	0.31		

and 375 nm bands, due to the R_1 and R_2 transitions of three associated F centers (F_3 center), the 520 and 545 nm bands, attributed to N_1 and N_2 transitions of the F_4 center, and the 632 nm band due to the F_2^+ center. The M-band spectral range is further overcrowded due to the presence of another broad absorption band, which appears as a shoulder of the M one on the short wavelength side and is ascribed to the presence of Li colloids [71]. The intensity at the peak wavelength of the M band increases monotonically with the irradiation dose, while that of the F band reaches a saturation value, after which a reduction starts. Using the Smakula formula [5] and assuming the defect density to be constant along the depth colored by the low-energy electrons, an average F concentration of $\sim 6.2 \times 10^{19}$ cm^{-3} and an F_2 one of $\sim 3.5 \times 10^{18}$ cm^{-3} was obtained for the crystal irradiated at the highest dose. A simple physical dipole-field interaction model [72], previously tested by direct comparison with ellipsometric measurements [73] and later extended to include Gaussian bands [74], was applied to quantitatively evaluate the single contributions of different kinds of electronic defects to the overall refractive index change of the colored volume of 12 keV electron irradiated CC waveguides [75]. The adopted model allows to estimate the contribution from each type of point defects to the modified complex refractive index of the irradiated layer: Fig. 5b shows the cumulative dispersion of refractive index for the CC waveguide irradiated at the highest dose, along with the partial contributions from the various absorption bands due to aggregate CCs. The total increase of the refractive index amounts to about 4 % with respect to the uncolored value at 633 nm, that is, where the F_2 visible emission band is located. It is shown that the main contribution to the refractive index change at longer wavelengths is due to the F centers, that absorb light in the UV range. Its amount is comparable to that due to the presence of strong, almost overlapping F_2 and F_3^+ absorption bands. The conspicuous modification is not surprising, as the concentration of the produced defects results $\sim 10^{20}$ cm^{-3}, compared to 6.1×10^{22} halogen sites/cm^3 in the LiF lattice.

It is evident in Fig. 5a that, at high doses, the role of more complex and larger aggregate defects, such as the F_4 centers, is not negligible. As

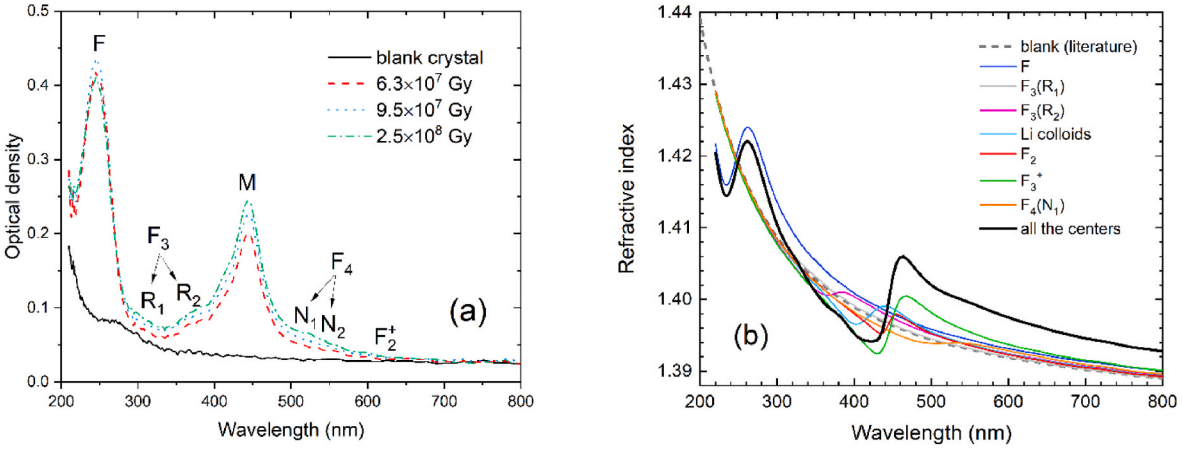


Fig. 5. Optical absorption spectra of the three CC waveguides written on a LiF crystal by irradiation with 12 keV electrons at increasing doses. The measured spectrum of an untreated zone of the crystal is also shown for comparison (a). Refractive index (black, thick solid line) of the CC LiF waveguide irradiated at the highest dose as deduced from the best fit of its transmittance spectrum. The partial contributions of several types of CCs are shown. The refractive index of uncolored bulk LiF (dashed line) is reported for comparison (b).

a matter of fact, the absorption of these defects considerably increases the extinction coefficient in the green spectral region, where the F_3^+ emission is located, introducing significant optical losses at these wavelengths. Indeed, the increase in the extinction coefficients at 540 nm is about five times greater than in the red, at 670 nm. The higher losses, together with the existence of a triplet state in the optical cycle of the F_3^+ CCs [75], can explain the absence of a gain in the green spectral range. On the contrary, the net optical gain coefficients of several cm^{-1}, measured in the red at the F_2 lasing wavelengths (see Fig. 4b), demonstrate that in these single-mode waveguides, based on CCs and produced by low-energy electron irradiation of LiF crystals, the irradiation conditions are suitable for the realization of amplifiers and lasers. Due to the high concentrations of F_2 defects, the intrinsic gain overcomes losses caused by re-absorption phenomena of more complex aggregate defects, while the waveguiding configuration lowers the laser threshold.

3. Color center waveguides in LiF crystals by He^+ ion irradiation

The realization of multi-mode CC waveguides in LiF crystals by irradiation with a 1.1 MeV He^+ beam at normal incidence was reported for different ion fluences varying from 1×10^{12} to 6×10^{15} cm^{-2}, producing colored stripes about 3.7 μm thick [26]. The formation of CCs was confirmed by optical absorption spectra, from which very high-volume concentrations of the F (~3×10^{20} cm^{-3}) and F_2 (~4×10^{19} cm^{-3}) CCs were evaluated at the highest doses. The presence of several dark lines in all the samples was observed as proof of guided propagation. For the samples irradiated with the fluence of 1×10^{14} cm^{-2}, the induced change in the refractive index was estimated to be about 1 % and values of ~1.5 dB/cm were found for propagation losses measured at 635 nm.

Contrary to low-energy electrons, which mainly interact with electrons in solids, the peculiar interaction of ions with matter can substantially modify the host matrix by atom displacement. Besides generation of point defects, other phenomena can take place and possibly become predominant. To better understand this complex behavior and take advantage of the high versatility offered by ion implantation [76], six broad-band visible-emitting planar waveguides were produced in LiF crystals irradiated at increasing doses with 1.5 and 2 MeV He^+ ions, as listed in Table 3.

Accurate m-line spectroscopy measurements and systematic mode analysis [27] allowed the full reconstruction of the complex depth refractive index profiles at 632.8 nm, which are shown in Fig. 6a and b, at the energies of 1.5 and 2 MeV, respectively, for the six planar waveguides. In the figures, the ion energy loss, evaluated with the Monte Carlo software SRIM [77], is superimposed. It increases as the projectile penetrates the solid and reaches its maximum at about half of its range (see also Table 3). Although the ranges in LiF are quite different at the two energies, the mean energy losses are practically the same.

The refractive index profiles shown in Fig. 6 are ascribable to the coexistence of two competitive physical mechanisms, associated with different processes of energy deposition along the ion track, responsible for positive and negative modifications of the refractive index. The first mechanism is an increase in refractive index due to the stable formation of high concentrations of primary and aggregate CCs in the *initial* part of the ion tracks, mainly due to the electronic interaction of ions with the crystal. Its effect is very similar to that observed in the CC waveguides written by low-energy electrons, see Fig. 5b. The second mechanism, which is essentially due to anelastic nuclear interactions, induces a reduction in material density and, consequently, in the refractive index, mainly in the *final* part of the ion tracks. This mechanism is particularly efficient at higher ion doses and is responsible for the formation of a buried negative index barrier at the end of the ion track, which helps to confine modes that possess an effective refractive index lower than the uncolored LiF substrate. Increasing the dose efficiently induces a larger and higher low-index barrier, which asymmetrically broadens the damaged region towards the surface. This asymmetry could be due to electronically induced migration of the defects formed by the nuclear collisions [76].

The energy loss profiles associated with these two processes, as obtained from SRIM simulations [77], are plotted in Fig. 7a for the case of 1.5 MeV ions. In this figure, the depth of the maximum in the nuclear interaction losses (black dashed line) practically coincides with that of the minimum of the refractive index in Fig. 6a. The superposition of single ion tracks and local damaging of the LiF matrix, besides reducing the material density, can also be accompanied by the formation of more complex defects, including nanometric lithium clusters [71], as confirmed by the optical absorption spectra shown in Fig. 7b.

Again, the main bands are due to F and M absorptions: at the three lowest doses, the spectra in Fig. 7b are similar to the absorption spectra in Fig. 5a, although the optical density values are higher due to the larger colored depths in the case of He^+ ions. Saturation is reached at doses higher than ~10^8 Gy, where the F and M maxima intensities start to decrease, and a more significant increase of spectral contributions from other types of more complex aggregate defects, together with those associated with sub-wavelength sized Li colloids, was observed. These metallic nanoaggregates are assumed to be spatially located mainly at the end of the ion tracks, where the nuclear damaging processes are more efficient (see Fig. 7a). Starting from the absorption spectra in Fig. 7b, a reliable quantitative spectral deconvolution, considering the peculiar energy loss vs. depth curve shown in Fig. 6, was performed [78] and used for evaluating the concentrations of the F and F_2 CCs. These resulted to be ~9.7×10^{19} cm^{-3} and ~3.8×10^{18} cm^{-3}, respectively, for the irradiation with 1.5 MeV He^+ ions at the dose of 2×10^8 Gy. These concentrations of CCs are similar to those found at the highest dose for low-energy electrons. Moreover, using the dipole-field interaction model previously tested for low-energy electrons [72,73], the spectral variation of the refractive index was estimated. In Fig. 8a, the increase in refractive index at the LiF crystal surface, calculated at the wavelength of 632.8 nm from the absorption spectra in Fig. 7b, is compared with that obtained from Fig. 6 as a function of the dose for the six waveguides. The refractive indices obtained with the two completely independent methods are mutually close at the lowest doses, sharing a similar behavior: as the dose increases from the lowest value, the surface refractive index increases until it starts saturating and then decreases, due to the increasing production of aggregate CCs mainly located in the initial part of the ion tracks. Note how the refractive index values deduced from the absorption spectra are significantly larger than the corresponding ones derived from the m-line analysis at the three higher doses. There is a reasonable explanation for this fact. Indeed, in the elaboration of the absorption spectra, the Δn is calculated from the variation in the extinction coefficient, Δk, through the already mentioned dipole-oscillator model, which establishes a relationship

Table 3
Irradiation parameters of CC planar waveguides realized in LiF crystals with He^+ ions.

Energy (MeV)	1.5			2.0		
Range in LiF (μm)	4.42			5.89		
Mean energy loss (keV/μm)	3.35×10^2			3.36×10^2		
Fluence (ions/cm²)	1×10^{15}	5×10^{15}	1×10^{16}	6×10^{13}	2.5×10^{14}	2.5×10^{16}
Mean dose (Gy)	2.0×10^8	1.0×10^9	2.0×10^9	1.2×10^7	5.1×10^7	5.1×10^9

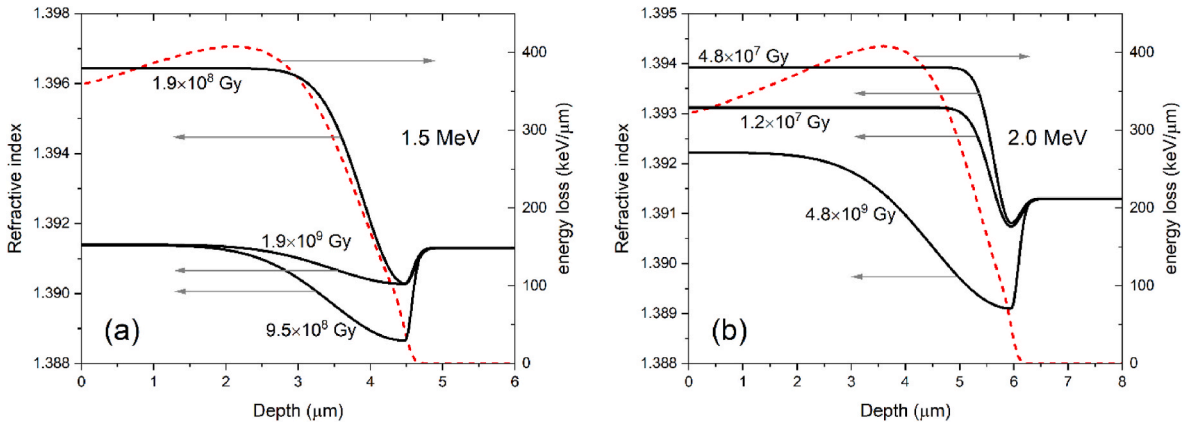


Fig. 6. Refractive index depth profiles (wavelength of 632.8 nm) as derived for planar waveguides in LiF crystals irradiated with He^+ at 1.5 (a) and 2 MeV (b) at three different ion doses with the method specified in the text. The ion linear energy losses (red dashed lines) are also reported. (For interpretation of the references to color in this figure legend, the reader is referred to the Web version of this article.)

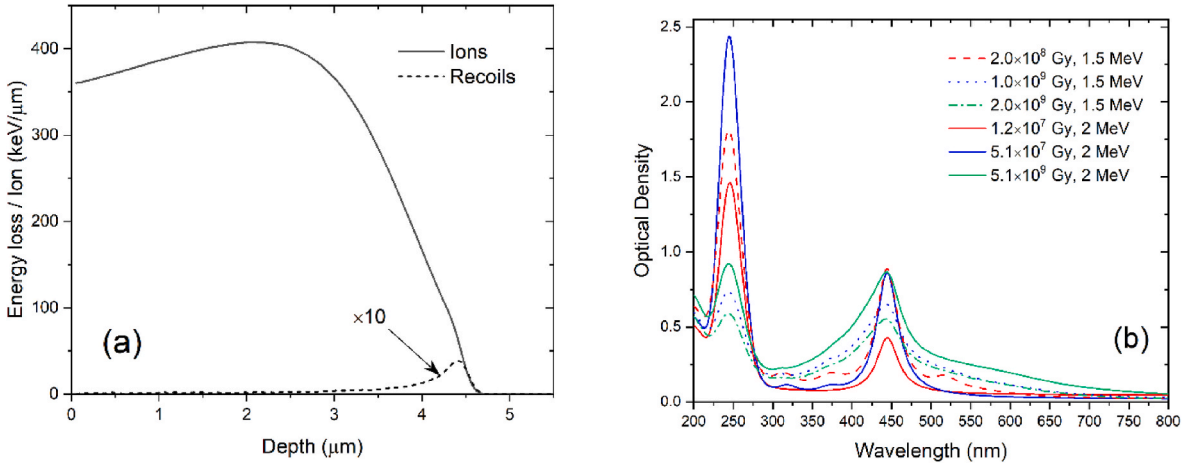


Fig. 7. Energy loss depth profiles of 1.5 MeV He^+ ions in LiF crystal for electronic (ions) and nuclear (recoils) processes as derived from SRIM simulations (a). Normal-incidence optical absorption spectra of the colored waveguides written on LiF crystals by He^+ at 1.5 MeV and 2 MeV (b).

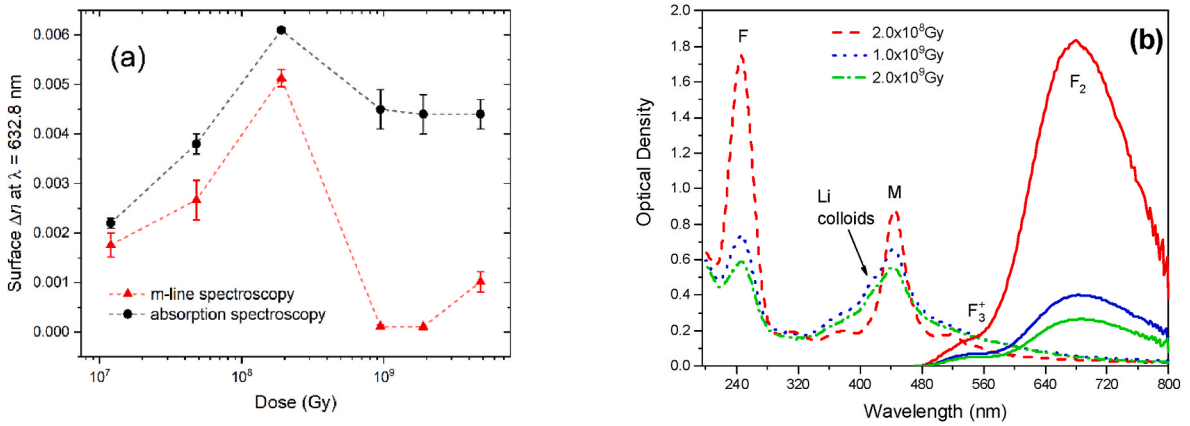


Fig. 8. Variation of the refractive index at the LiF crystal surface, as calculated with two completely independent methods (m-line and absorption spectroscopy, see the text), of the colored waveguides induced on LiF crystals irradiated with He^+ at 1.5 MeV and 2 MeV at increasing ion doses (a). Room temperature optical absorption (dashed lines) and PL spectra (solid lines) of three CC waveguides irradiated with He^+ at 1.5 MeV at increasing doses in a LiF crystal, measured under laser excitation at 457.9 nm (b).

between real and imaginary parts of the complex dielectric permeability of the irradiated volume. Variations in the refractive index as small as those estimated from the m-line analysis do not influence the absorption spectrum at all, which is, on the contrary, very sensible to variations in the extinction coefficient. In other words, the Δn calculated from the absorption spectra are related *only* to variations in the extinction

coefficient, on the other hand, the analysis of the m-line measurements allows one to evaluate variations in the refractive index due to *all* their possible causes, thus including both CC formation and ion-induced material density changes.

Regarding the emission properties, in Fig. 8b the PL spectra of the three CC waveguides irradiated with He^+ at 1.5 MeV at increasing doses are reported together with their optical absorption spectra. The monotonic decrease of the visible emission intensities of F_2 and F_3^+ CCs confirms a reduction of the concentrations of these electronic defects, mainly associated with the formation of Li colloids, whose absorption peak at ~410 nm is observed only at doses higher than 2×10^8 Gy.

To further explore the properties of the waveguides obtained by irradiation at 1.5 MeV, vibrational spectra were acquired using a DXR2xi Thermofisher Raman imaging Microscope. A depolarized 785 nm laser excitation was chosen to reduce fluorescence interference, using a power of about 28 mW and a 10x collection objective, to interrogate an overall depth of about 5 μm. Fig. 9a–b presents, respectively, the obtained Raman spectra for the high and low wavenumber regions. The three reported curves correspond to the regions irradiated with increasing doses and appearing with different shades of yellow, as visible in the inset of Fig. 9b, which shows the optical image of the irradiated crystal with increasing doses from right to left. The spectrum of a not irradiated sample is also reported as a comparison (black solid line).

As shown in Fig. 9a, the Raman intensity of the central band at about 1400 cm^{-1} increases significantly from the not irradiated to the lowest-dose colored area. This vibrational signature could be thus associated to the appearance of primary and aggregate CCs in the initial part of the ion tracks. However, when the critical dose of 10^9 Gy is reached, the band intensity begins to decrease and a separate shoulder appears that progressively moves towards the low wavenumbers for increasing doses, as evidenced by the inset of the figure showing a magnification of the central region of the spectra. A multi-peak fitting allowed to estimate a displacement of about 2 cm^{-1} for the appearing shoulder when passing from the central dose of 10^9 Gy to the highest dose. Given that a similar trend also occurs when acquiring Raman spectra on materials subjected to an increase in local temperature [79], the revealed behavior could be attributed to the density reduction of the LiF crystal induced by lattice damage, mainly at the end of the ion tracks. This is accompanied by a slight reduction in the efficiency of the primary and aggregate CC formation. Therefore, the identified shoulder at high doses could be ascribed to the formation of metallic colloids. Similarly, Fig. 9b demonstrates a specific modification of the Raman spectrum in the low wavenumber region with increasing doses. In fact, from the not irradiated to the lowest-dose colored area some peaks appear at about 350, 420 and 550 cm^{-1}. Following the density functional theory calculations reported in Ref. [80], these peaks can be associated to the initial formation of primary defects in the LiF matrix, such as F centers and halogen vacancies. After a further increase of the dose, some additional relevant contributions appear, first at about 600 cm^{-1}, and, for the higher dose, around 520 cm^{-1}, possibly due to the production of more complex aggregates. These interesting and novel results could pave the way for exploiting a simple and non-invasive vibrational approach in the analysis of defect formation in irradiated LiF crystals and thin films.

4. Conclusions

Radiation damage by light-ion or electron beams to certain insulating crystals induces the stable formation of CCs that are able to fluoresce and can be exploited as the active medium for photonic devices. LiF crystals can serve as the host for aggregate defects that emit in the green and red portions of the visible spectrum and can be fabricated in waveguide form. Electron beam lithography was used to write single-mode channel waveguides on the surface of optically polished LiF crystals. When excited with a laser line at 457.9 nm, the waveguides exhibited ASE in a broad band centered at 650 nm with gain coefficients of several cm^{-1}. The quantitative results obtained on the guiding and amplifying properties are suitable for the realization of low-threshold tunable miniaturized amplifiers and lasers operating in the visible spectrum, even in continuous regime. At the selected energies and doses, in a single-step process, it was demonstrated that the direct e-beam writing technology is suitable for fabricating CC waveguides in LiF crystals, despite the material insulating nature. Considering the limited penetration depth of low-energy electrons, further developments can be foreseen using LiF films as host for laser-active CCs. Moving to light-ion beams, like He^+ and, more recently, C^+, the peculiar and more complex interactions with the lattice and the higher ranges pave the way for the realization of single-mode CC waveguides also in the near-infrared spectral range, where stable broadly tunable lasers based on other types of aggregate defects efficiently operate in doped LiF crystals. The opportunities offered by the choice of ion mass and energy along with a better understanding of radiation-matter interactions, are promising for finding suitable irradiation conditions, overcoming the technological challenge of CC waveguide lasers and amplifiers operating in the visible and also in the near-infrared.

CRediT authorship contribution statement

Rosa Maria Montereali: Writing – original draft, Validation, Supervision, Methodology, Investigation, Conceptualization. **Valentina**

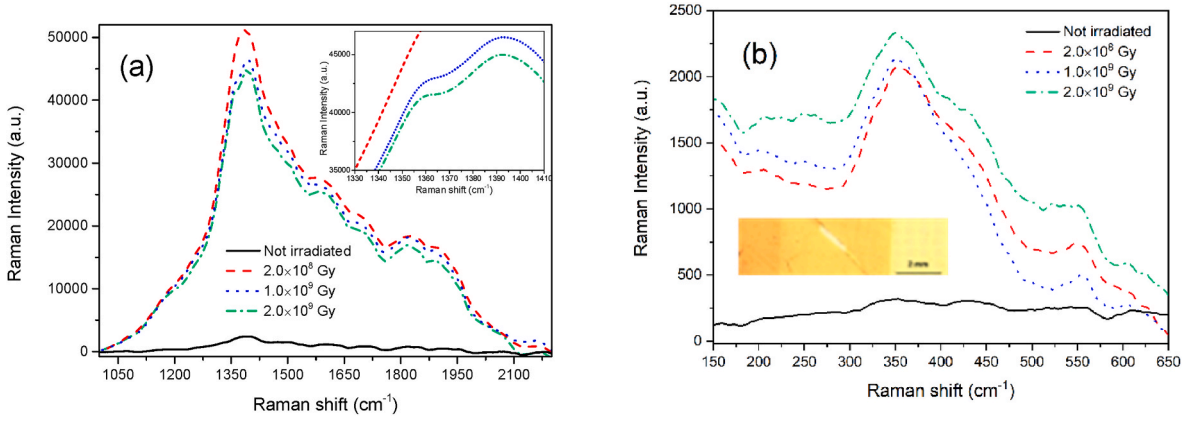


Fig. 9. Raman spectra of the CC waveguides obtained by He^+ irradiation at 1.5 MeV and three different doses, in the high wavenumber region (a) and the low wavenumber region (b). The inset in Fig. 9a is a magnification of the central region to evidence the slight shift of the peaks with increasing dose. The inset in Fig. 9(b) shows the optical image of the crystal irradiated with increasing doses from right to left. The spectrum of a not irradiated sample is also reported as a comparison (black solid line).

Mussi: Writing – review & editing, Methodology, Investigation, Data curation. **Enrico Nichelatti:** Writing – review & editing, Visualization, Software, Formal analysis, Data curation. **Massimo Piccinini:** Writing – review & editing, Validation, Investigation, Data curation.

Declaration of competing interest

The authors declare that they have no known competing financial interests or personal relationships that could have appeared to influence the work reported in this paper.

Acknowledgements

The authors are indebted with many valuable colleagues, researchers, technicians, students, and guests, whose contributions are cited in the reference list.

Data availability

Data will be made available on request.

References

[1] E.D. Palik, Handbook of Optical Constants of Solids, Academic Press, New York, 1997, 98. ISBN 0125444230.
[2] M. Piacentini, A new interpretation of the fundamental exciton region in LiF, Solid State Commun. 17 (6) (1975) 697–700, https://doi.org/10.1016/0038-1098(75)90388-9.
[3] K. Maesh, P.S. Weng, C. Furetta, Thermoluminescence in Solids and its Applications, NTP, England, UK, 1989. ISBN 1870965019.
[4] S.W.S. McKeever, A Course in Luminescence Measurements and Analyses for Radiation Dosimetry, first ed., Wiley, 2022. ISBN 978-1-119-64692-1.
[5] W.B. Fowler, Physics of Color Centers, Academic Press, New York and London, 1968.
[6] N. Itoh, M. Stoneham, Materials Modification by Electronic Excitation, Cambridge University Press, Cambridge, UK, 2001. ISBN 0 521 55498 5.
[7] J. Nahum, Optical properties and mechanism of formation of some F-aggregate centers in LiF, Phys. Rev. 158 (1967) 814–825, doi.org/814.10.1103/PhysRev.158.814.
[8] G. Baldacchini, E. De Nicola, G. Giubileo, F. Menchini, G. Messina, R. M. Montereali, A. Scacco, Selective production of aggregate centers in LiF crystals by ionizing radiations, Nucl. Instrum. Methods B 141 (1998) 542–546.
[9] G. Baldacchini, E. De Nicola, R.M. Montereali, A. Scacco, V. Kalinov, Optical bands of F_2 and F_3^+ centers in LiF, J. Phys. Chem. Solid. 61 (2000) 21–26, https://doi.org/10.1016/S0022-3697(99)00236-X.
[10] K. Schwartz, J. Maniks, I. Manika, A review of colour center and nanostructure creation in LiF under heavy ion irradiation, Phys. Scripta 90 (9) (2015) 094011, https://doi.org/10.1088/0031-8949/90/9/094011.
[11] A.P. Voitovich, V.S. Kalinov, Y.V. Loiko, N.N. Naumenko, L.P. Runets, A.P. Stupak, Spatial structures based on color centers created by electrons in lithium fluoride crystals: absorption and luminescence characteristics, J. Appl. Spectrosc. 75 (2008) 104–113, https://doi.org/10.1007/s10812-008-9006-9.
[12] M.V. Sorokin, ZhB. Malikova, A.K. Dauletbekova, G. Baubekova, G.M. Aralbayeva, A.T. Akilbekov, Thermal annealing of radiation damages produced by swift ^{14}N and ^{16}O ions in LiF crystals, Mater. Res. Express 11 (7) (2024) 076201, https://doi.org/10.1088/2053-1591/ad5a68.
[13] T.T. Basiev, S.B. Mirov, V.V. Osiko, Room-temperature color center lasers, IEEE J. Quant. Electron. 24 (1988) 1052–1069, https://doi.org/10.1109/3.229.
[14] W. Gellermann, Color center lasers, J. Phys. Chem. Solid. 52 (1) (1991) 249–297, https://doi.org/10.1016/0022-3697(91)90068-B.
[15] V.V. Ter-Mikirtychev, T.T. Tsuboi, Stable room-temperature tunable color center lasers and passive Q-switchers, Prog. Quant. Electron. 20 (3) (1996) 219–268, https://doi.org/10.1016/0079-6727(96)00001-8.
[16] L.X. Zheng, L.F. Wan, Double stimulated emission of mixed color centers in LiF crystal, Opt Commun. 55 (1985) 277–279.
[17] Y.L. Gusev, S.N. Konoplin, S.I. Marennikov, Generation of coherent radiation in F_2 color centers in an LiF single crystal, Sov. J. Quant. Electron. 7 (1977) 1157–1158, https://doi.org/10.1070/QE1977v007n09ABEH012826.
[18] G. Baldacchini, M. Cremona, R.M. Montereali, L.C. Scavarda do Carmo, R. A. Nunes, S. Paciornik, F. Somma, V. Kalinov, Photoluminescence of LiF crystal colored by focused electron beam, Opt Commun. 94 (1992) 139–142, https://doi.org/10.1016/0030-4018(92)90422-N.
[19] R.M. Montereali, A. Mancini, G.C. Righini, S. Pelli, Active stripe waveguides produced by electron beam lithography in LiF crystals, Opt Commun. 153 (1998) 223–225.
[20] R.M. Montereali, G. Baldacchini, L.C. Scavarda do Carmo, LiF films: absorption and luminescence of colour centres, Thin Solid Films 201 (1991) 106–108.
[21] G.C. Righini, S. Pelli, R.M. Montereali, S. Martelli, A. Mancini, L. Fornarini, G. Baldacchini, Passive and active optical waveguides in LiF thin films, in: G. C. Righini, S.I. Najafi, B. Jalali (Eds.), Integrated Optic Devices II, Proceedings of SPIE, vol. 3278, 1998, pp. 132–138, https://doi.org/10.1117/12.298192.
[22] R.M. Montereali, S. Martelli, G.C. Righini, S. Pelli, C.N. Afonso, A. Perea, D. Barbier, P. Bruno, Perspectives of application of alkali fluoride films in integrated optical circuits, in: P. Vincenzini, G.C. Righini (Eds.), 9th CIMTEC-World Forum on New Materials, Symposium X - Innovative Light Emitting Materials, Techna s.r.L, 1999, pp. 321–328.
[23] R.M. Montereali, Point defects in thin insulating films of lithium fluoride for optical microsystems, in: H.S. Nalwa (Ed.), Handbook of Thin Film Materials, vol. 3, Ferroelectric and Dielectric Thin Films, Academic Press, 2002, pp. 399–431. Ch.7, ISBN: 0125129084, 9780125129084.
[24] R.M. Montereali, M. Piccinini, E. Burattini, Amplified spontaneous emission in active channel waveguides produced by electron beam lithography in LiF crystals, Appl. Phys. Lett. 78 (26) (2001) 4082–4084, https://doi.org/10.1063/1.1381568.
[25] R.M. Montereali, M. Piccinini, Optical gain of F_2 colour centres in LiF confining structures realised by electron-beam lithography, Opt Commun. 209 (2002) 201–208, https://doi.org/10.1016/S0030-4018(02)01631-0.
[26] M. Cremona, J.A.M. Pereira, S. Pelli, G.C. Righini, Optical waveguides produced in LiF by MeV ion beam bombardment, Appl. Phys. Lett. 81 (2002) 4103–4105, https://doi.org/10.1063/1.1524302.
[27] V. Mussi, F. Somma, P. Moretti, J. Mugnier, B. Jacquier, R.M. Montereali, E. Nichelatti, Mode analysis in He^+-Implanted lithium fluoride planar waveguides, Appl. Phys. Lett. 82 (22) (2003) 3886–3888, https://doi.org/10.1063/1.1577822.
[28] V. Mussi, R.M. Montereali, P. Moretti, J. Mugnier, E. Nichelatti, F. Somma, B. Jacquier, Active waveguides produced in lithium fluoride by He^+ implantation, Nucl. Instrum. Methods B 230 (2005) 257–261, https://doi.org/10.1016/j.nimb.2004.12.051.
[29] R.M. Montereali, P. Moretti, V. Mussi, J. Mugnier, E. Nichelatti, F. Somma, B. Jacquier, Optical characterization of active waveguides produced in lithium fluoride by He^+ implantation, in: H.J. Kalinowski, M.A. Romero, S.E. Barbin (Eds.), Proc. SBMO/IEEE MTT-S International Microwave and Optoelectronics Conference - IMOC, 2003, pp. 447–451. ISBN 0-7803-7824-5.
[30] J.A.M. Pereira, M. Cremona, S. Pelli, E.L.A. Macchione, K. Koide, S.S. Vasconcelos, G.C. Righini, Nucl. Instrum. Methods B 240 (2005) 234–238, https://doi.org/10.1016/j.nimb.2005.06.122.
[31] L. Zhang, M. Zhu, Z. Zhang, Y. Wang, J. Xiao, Near-infrared single-mode optical waveguide fabrication in LiF crystal by carbon ion irradiation, Jpn. J. Appl. Phys. 61 (2022) 070903, https://doi.org/10.35848/1347-4065/ac74fd.
[32] A. Belarouci, F. Menchini, H. Rigneault, B. Jacquier, R.M. Montereali, F. Somma, P. Moretti, M. Cathelinaud, Control of F_2 color centers spontaneous emission in LiF thin films inside optical microcavities, Opt. Mater. 16 (2001) 63–67, https://doi.org/10.1016/S0925-3467(00)00060-4.
[33] R. Saoudi, A. Belarouci, P. Moretti, B. Jacquier, H. Rigneault, M. Cathelinaud, E. Nichelatti, R.M. Montereali, F. Somma, Engineering of optical active microcavities based on color centers in LiF by ion implantation, Opt. Mater. 28 (2006) 1166–1170, https://doi.org/10.1016/j.optmat.2005.07.010.
[34] S.K. Sekatskii, G. Dietler, F. Bonfigli, S. Loreti, T. Marolo, R.M. Montereali, Subwavelength-size local fluorescent sources based on color centers in LiF for scanning near-field optical microscopy, J. Lumin. 122–123 (2007) 362–364, https://doi.org/10.1016/j.jlumin.2006.01.190.
[35] V. Mussi, F. Granone, T. Marolo, R.M. Montereali, C. Boragno, F. Buatier de Mongeot, U. Valbusa, Surface nanostructuring and optical activation of lithium fluoride crystals by ion beam irradiation, Appl. Phys. Lett. 88 (2006) 103116–103118, https://doi.org/10.1063/1.2177660.
[36] V.P. Dresvyanskiy, S.A. Zilov, E.F. Martynovich, Fluctuating fluorescence of single color centers in lithium fluoride crystals, Opt. Spectrosc. 131 (2023) 365–372, https://doi.org/10.1134/S0030400X23020066.
[37] G. Baldacchini, F. Bonfigli, F. Flora, R.M. Montereali, D. Murra, E. Nichelatti, A. Faenov, T. Pikuz, High-contrast photoluminescent patterns in lithium fluoride crystals produced by soft x-rays from a laser-plasma source, Appl. Phys. Lett. 80 (2002) 4810–4812, https://doi.org/10.1063/1.1486476.
[38] G. Baldacchini, F. Bonfigli, A. Faenov, F. Flora, R.M. Montereali, A. Pace, T. Pikuz, L. Reale, Lithium fluoride as a novel X-ray image detector for biological μ-world capture, J. Nanosci. Nanotechnol. 3 (2003) 483–486, https://doi.org/10.1166/jnn.2003.023.
[39] F. Bonfigli, A. Faenov, F. Flora, M. Francucci, P. Gaudio, A. Lai, S. Martellucci, R. M. Montereali, T. Pikuz, L. Reale, M. Richetta, M.A. Vincenti, G. Baldacchini, High-resolution water window X-ray imaging of in vivo cells and their products using LiF crystal detectors, Microsc. Res. Tech. 71 (2008) 35–41, https://doi.org/10.1002/jemt.20523.
[40] T. Pikuz, A. Faenov, Y. Fukuda, M. Kando, P. Bolton, A. Mitrofanov, A. Vinogradov, M. Nagasono, H. Ohashi, M. Yabashi, K. Tono, Y. Senba, T. Togashi, T. Ishikawa, Optical features of a LiF crystal soft x-ray imaging detector irradiated by free electron laser pulses, Opt Express 20 (4) (2012) 3424–3433, https://doi.org/10.1364/OE.20.003424.
[41] T. Kurobori, A. Matoba, Development of accurate two-dimensional dose-imaging detectors using atomic-scale color centers in Ag-activated phosphate glass and LiF thin films, Jpn. J. Appl. Phys. 53 (2014), https://doi.org/10.7567/JJAP.53.02BD14, 02BD.
[42] P. Estrela, E. Maçôas, G. Williams, M. Hussain, M. Fajardo, Lithium fluoride detectors for high spatial resolution imaging of tabletop XUV from high harmonic generation in gases, J. Opt. Soc. Am. B 38 (7) (2021) 2234, https://doi.org/10.1364/JOSAB.422767.
[43] R.M. Montereali, F. Bonfigli, E. Nichelatti, M. Piccinini, M.A. Vincenti, Luminescence of point defects in lithium fluoride thin layers for radiation imaging detectors at the nanoscale, in: A.J. Meixner, M. Fleischer, D.P. Kern, E. Sheremet,

N. McMillan (Eds.), Optical NanoSpectroscopy, Applications, vol. 3, De Gruyter, Berlin, Boston, 2023, pp. 69–96, https://doi.org/10.1515/9783110442908-005. ISBN: 9783110442908.
[44] M. Piccinini, F. Ambrosini, A. Ampollini, M. Carpanese, L. Picardi, C. Ronsivalle, F. Bonfigli, S. Libera, M.A. Vincenti, R.M. Montereali, Solid state detectors based on point defects in lithium fluoride for advanced proton beam diagnostics, J. Lumin. 156 (2014) 170–174, https://doi.org/10.1016/j.jlumin.2014.08.008.
[45] M. Piccinini, E. Nichelatti, A. Ampollini, L. Picardi, C. Ronsivalle, F. Bonfigli, S. Libera, M.A. Vincenti, R.M. Montereali, Proton beam dose-mapping via color centers in LiF thin film detectors by fluorescence microscopy, Europhys. Lett. 117 (2017), https://doi.org/10.1209/0295-5075/117/37004, 37004-1-5.
[46] E. Nichelatti, M. Piccinini, A. Ampollini, L. Picardi, C. Ronsivalle, F. Bonfigli, M. A. Vincenti, R.M. Montereali, Bragg-curve imaging of 7 MeV protons in a lithium fluoride crystal by fluorescence microscopy of colour centres, Europhys. Lett. 120 (2017), https://doi.org/10.1209/0295-5075/120/56003, 56003-1-5.
[47] R.M. Montereali, V. Nigro, M. Piccinini, M.A. Vincenti, A. Ampollini, P. Nenzi, C. Ronsivalle, E. Nichelatti, Bragg curve detection of low-energy protons by radiophotoluminescence imaging in lithium fluoride thin films, Sensors 23 (2023) 4779, https://doi.org/10.3390/s23104779.
[48] M. Piccinini, E. Nichelatti, M.A. Vincenti, V. Nigro, C. Ronsivalle, A. Ampollini, P. Nenzi, G. Bazzano, E. Trinca, R.M. Montereali, Dynamic range and dose linearity of the radiophotoluminescence intensity in lithium fluoride crystals irradiated with 2.3 and 26 MeV protons, J. Lumin. 259 (2023) 119833, https://doi.org/10.1016/j.jlumin.2023.119833.
[49] M. Piccinini, E. Nichelatti, A. Ampollini, G. Bazzano, C. De Angelis, S. Della Monaca, P. Nenzi, L. Picardi, C. Ronsivalle, V. Surrenti, E. Trinca, M. Vadrucci, M. A. Vincenti, R.M. Montereali, Dose response and Bragg curve reconstruction by radiophotoluminescence of color centers in lithium fluoride crystals irradiated with 35 MeV proton beams from 0.5 to 50 Gy, Radiat. Meas. 133 (2020) 106275, https://doi.org/10.1016/j.radmeas.2020.106275, 1-4.
[50] M. Piccinini, A. Mirandola, V. Nigro, M.A. Vincenti, M. Ciocca, R.M. Montereali, Radiophotoluminescence response of LiF:Mg,Ti pellets irradiated with clinical proton beams in the 70-200 MeV energy range, Radiat. Meas. 174 (2024) 107153, https://doi.org/10.1016/j.radmeas.2024.107153.
[51] E. Nichelatti, M. Piccinini, A. Ampollini, L. Picardi, C. Ronsivalle, F. Bonfigli, M. A. Vincenti, R.M. Montereali, Modelling of photoluminescence from F_2 and F_3^+ colour centres in lithium fluoride irradiated at high doses by low-energy proton beams, Opt. Mater. 89 (2019) 414–418, https://doi.org/10.1016/j.optmat.2019.01.052.
[52] P. Bilski, B. Marczewska, Fluorescent detection of single tracks of alpha particles using lithium fluoride crystals, Nucl. Instrum. Methods Phys. Res. Sect. B Beam Interact. Mater. Atoms 392 (2017) 41–45, https://doi.org/10.1016/j.nimb.2016.12.003.
[53] P. Bilski, B. Marczewska, W. Gieszczyk, M. Kłosowski, T. Nowak, M. Naruszewicz, Lithium fluoride crystals as fluorescent nuclear track detectors, Radiat. Protect. Dosim. 178 (2018) 337–340, https://doi.org/10.1093/rpd/ncx116.
[54] M. Sankowska, P. Bilski, B. Marczewska, Thermal enhancement of the intensity of fluorescent nuclear tracks in lithium fluoride crystals, Radiat. Meas. 157 (2022) 106845, https://doi.org/10.1016/j.radmeas.2022.106845.
[55] M. Piccinini, E. Nichelatti, G. Esposito, E. Cisbani, V. Nigro, M.A. Vincenti, F. Limosani, C. Ronsivalle, A. Ampollini, C. De Angelis, R.M. Montereali, Detection of fluorescent low-energy proton tracks in lithium fluoride crystals, Radiat. Meas. 174 (2024) 206701, https://doi.org/10.1016/j.radmeas.2024.107140.
[56] V. Nigro, C. Colantonio, M. Piccinini, E. Buratti, R. Ciciotti, E. Cisbani, C. De Angelis, F. Dinelli, G. Esposito, F. Limosani, E. Nichelatti, C. Ronsivalle, M. A. Vincenti, B. Ruzicka, R.M. Montereali, PNIPAM microgel coatings of LiF crystal radiation detectors, Colloids and Surfaces A Physicochemical and Engineering Aspects 702 (2024) 135105, https://doi.org/10.1016/j.colsurfa.2024.135105.
[57] M. Sankowska, P. Bilski, M. Kłosowski, A. Kilian, W. Gieszczyk, B. Marczewska, Isotopically enriched lithium fluoride crystals for detection of neutrons with the fluorescent track technique, Materials 17 (20) (2024) 5029, https://doi.org/10.3390/ma17205029.
[58] X. Lu, L. Chang, M.A. Tran, T. Komljenovic, J.E. Bowers, K. Srinivasan, Emerging integrated laser technologies in the visible and short near-infrared regimes, Nat. Photonics 18 (10) (2024) 1010–1023, https://doi.org/10.1038/s41566-024-01529-5.
[59] S. Castelletto, M. Agio, Diamond colour centre enables an atomic optical antenna, Nat. Photonics 18 (10) (2024) 1004–1005, https://doi.org/10.1038/s41566-024-01522-y.
[60] L. Fornarini, S. Martelli, A. Mancini, R.M. Montereali, S. Pelli, G.C. Righini, Realization and characterization of broad-band active stripe waveguides in LiF films, in: Proceedings of the 9th European Conference on Integrated Optics, ECIO'99, Turin, Italy, 1999, pp. 343–346.
[61] R.A. Nunes, S. Paciornik, L.C. Scavarda do Carmo, H.J. Kalinowski, Electron-beam production of colour centres on alkali halide crystals and films, Nucl. Instrum. Methods Phys. Res. B 32 (N. 1–4) (1988) 222–224, https://doi.org/10.1016/0168-583X(88)90213-3.
[62] C.A. Andersen, in: T.D. McKinley, K.F. Heinrich, D.B. Wittry (Eds.), The Electron Microprobe, John Wiley, New York, 1964.
[63] A.E. Hughes, D. Pooley, H.U. Rahman, W.A. Runciman, Atomic Energy Research Establishment, Harwell, Berkshire, England, 1967. Report No. R 5604.
[64] A. Yariv, Quantum Electronics, third ed., John Wiley & Sons, New York, 1987. Ch. 8. ISBN 978-0-471-60997-1.
[65] M. Olivier, in: D.B. Ostrowsky, E. Spitz (Eds.), New Directions in Guided Wave and Coherent Optics, NATO ASI Series: Applied Sciences, vol. 2, 1984, pp. 639–658. M. Nijhoff ISBN 9024729386.
[66] R.M. Montereali, A. Mancini, S. Martelli, F. Menchini, P. Picozzi, Micro and sub-micro fabrication techniques for optically confined structures based on lithium fluoride, Appl. Organomet. Chem. 15 (2001) 407–413, https://doi.org/10.1002/aoc.162.
[67] A.P. Voitovich, V.S. Kalinov, O.E. Kostik, A.N. Novikov, L.V. Simonchik, Radiation defect formation in lithium fluoride nanocrystals and crystals in an atmospheric-pressure glow discharge, J. Appl. Spectrosc. 90 (5) (2023) 995–999, https://doi.org/10.1007/s10812-023-01624-5 (Russian Original Vol. 90, No. 5, September–October 2023).
[68] Piccinini Massimo, Difetti puntiformi in film di fluoruro alcalini per dispositivi ottici integrati, Tesi di laurea, Università di Roma "La Sapienza,", 2000.
[69] G. Baldacchini, S. Bigotta, R.M. Montereali, Emission decay times of F_2 color centers in heavily irradiated LiF crystals, J. Lumin. 94–95 (2001) 299–303, https://doi.org/10.1016/S0022-2313(01)00309-X.
[70] M. Montecchi, E. Nichelatti, R.M. Montereali, M. Piccinini, F. Somma, Increase of refractive index induced by absorbing centres: homogeneous and inhomogeneous line-broadening cases, Opt. Quant. Electron. 36 (2004) 43–55, https://doi.org/10.1023/B:OQEL.0000015629.89080.84.
[71] L.H. Abu Hassan, P.D. Townsend, Ion implantation in LiF to form F and F_2 centres, J. Phys. C Solid State Phys. 19 (1986) 99–110, https://doi.org/10.1088/0022-3719/19/2/007.
[72] M. Montecchi, E. Nichelatti, A. Mancini, R.M. Montereali, Optical characterization of low-energy electron-beam-colored LiF crystals by spectral trasmittance measurements, J. Appl. Phys. 86 (6) (1999) 3745–3750, https://doi.org/10.1063/1.371245.
[73] M. Montecchi, R.M. Montereali, E. Nichelatti, Refractive index modification from colour centres in dielectric confining structures, Opt. Mater. 17 (2001) 347–350, https://doi.org/10.1016/S0925-3467(01)00059-3.
[74] R.M. Montereali, F. Bonfigli, M. Montecchi, E. Nichelatti, M. Piccinini, Advanced optical characterization of broad-band light-emitting color-center strip waveguides in lithium fluoride, in: G.C. Righini, S.K. Honkanen, L. Pavesi, L. Vivien (Eds.), Silicon Photonics and Photonic Integrated Circuits, Proceedings of SPIE, vol. 6996, 2008, 69960J_1-9.
[75] G. Baldacchini, M. Cremona, G. d'Auria, R.M. Montereali, V. Kalinov, Radiative and nonradiative processes in the optical cycle of the F_3^+ center in LiF, Phys. Rev. B 54 (24) (1996) 17508–17514, https://doi.org/10.1103/physrevb.54.17508.
[76] P.D. Townsend, P.J. Chandler, L. Zhang, Optical Effects of Ion Implantation, Cambridge University Press, 1994, https://doi.org/10.1017/CBO9780511599781.
[77] J.F. Ziegler, M.D. Ziegler, J.P. Biersac, SRIM - the stopping and range of ions in matter (2010), Nucl. Instrum. Methods B 268 (2010) 1818–1823, https://doi.org/10.1016/j.nimb.2010.02.091.
[78] F. Bonfigli, B. Jacquier, R.M. Montereali, P. Moretti, V. Mussi, E. Nichelatti, F. Somma, Concentration of F_2 and F_3^+ defects in He^+ implanted LiF crystals determined by optical transmission and photoluminescence measurements, Opt. Mater. 24 (2003) 291–296, https://doi.org/10.1016/S0925-3467(03)00137-X.
[79] A. Valletta, V. Mussi, M. Rapisarda, A. Lucibello, M. Natali, M. Peroni, C. Lanzieri, G. Fortunato, L. Mariucci, Hybrid electrothermal simulations of GaN HEMT devices based on self-heating free virtual electrical characteristics, IEEE Trans. Electron. Dev. 68 (2021) 3740, https://doi.org/10.1109/TED.2021.3084547.
[80] A.V. Sorokin, S. Piskunov, I. Isakoviča, I. Makarenko, I. Karbovnyk, A.I. Popov, Raman spectra of vacancy-containing LiF: predictions from first principles, Nuclear Inst, Methods in Physics Research B 480 (2020) 33, https://doi.org/10.1016/j.nimb.2020.07.025.